Electrical-based Condition Monitoring Using Shaft Speed Oscillation Harmonics

Uzoma Orji, Christopher Schantz, Darrin E. Barber, Dr. Steven B. Leeb, Dr. Robert Cox, LT J. Andrew Goshorn, ENS Kevin Thomas

***Abstract*—This paper proposes a method for electrical-based condition monitoring using shaft speed oscillation harmonics to assess the health of an electrical load. Experimental results have shown that the frequency content of these harmonics correlate well with readings from a handheld vibration meter. An algorithm is proposed to monitor the health of multiple motors from one aggregate current signal. The experimental results have shown the effectiveness of such a method but certain limitations exist and are discussed in this paper. This paper will also discuss how other frequency content, specifically bearing frequencies, can be used in future work to assess the health of motors in the laboratory setting but also in the field. Possible limitations to using these bearing frequencies are also discussed.**

I. Introduction

The United States Coast Guard uses vibration analysis to assess a particular electric machine's condition such as bearing faults, misalignment, imbalance, electrical faults and several other potentially damaging faults [1]. The current method of vibration monitoring requires mounting a sensor to the outer hub of the motor and taking readings from a hand-held vibration meter. One concern with this method involves the position of the transducer that is placed on the outer hub. A preliminary study by Thomson et al. [2] showed that stator frame vibration changes as a function of the transducer position around the periphery of the frame. There is no guarantee that the transducer will be placed at the same location each time there is a maintenance check. The accuracy of these readings over time may not be as reliable as they ought to be. Also, the method requires manned inspection and may be costly. Finally, these vibration checks are conducted periodically which may not be frequent enough to catch any serious, potentially fatal, damage in a motor.

Electrical-based vibration monitoring could overcome some of these shortcomings. By monitoring the current drawn by the motor, the data recorded are less prone to operator error. Electrical-based monitoring can be automated so that a computer can track the vibration of the motor more regularly. Finally, electrical-based vibration monitoring might eliminate the need for outside experts as the analysis can be done "in-house" by a computer.

This paper reviews a method that can track vibration on a motor using only electrical signals.

II. Shaft Speed Oscillation Harmonics

To begin developing a model to predict the location of shaft speed oscillation harmonics in the motor current spectrum, a simplified steady-state equivalent circuit is used to model an induction motor. The following derivation is adapted from [3]. The equivalent circuit includes only a slip-dependent rotor resistance as shown in Fig 1.

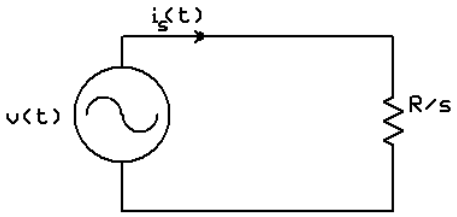

Fig. 1. Simplified steady-state equivalent circuit model of motor containing only a voltage source and a slip-dependent rotor resistance. The location of the shaft speed oscillation harmonics can be determined by fully expressing the stator current $i_s(t)$.

The shaft speed of the motor is assumed to be comprised of an average speed and a sinusoidally-varying component given by Eq. (1).

$$n(t) = N_r + \sum_k N_k \sin\left(2\pi k f_c t\right), \tag{1}$$

where N_r is the motor's rotational speed in rotations per minute, N_k are the Fourier components of the speed fluctuation, and f_c is fundamental frequency of the speed fluctuation, The rotational speed N_r can be calculated as

$$N_r = \frac{60}{p} \cdot \frac{\omega_r}{2\pi}, \tag{2}$$

where ω_r is the rotational frequency in radians per second and p is the number of pole pairs. The relative phases between the sinusoids are ignored in this derivation.

The line voltage is modeled as a pure sine wave at the line frequency, given by Eq. (3).

$$v(t) = V \sin\left(2\pi f t\right), \tag{3}$$

where V is the voltage amplitude, and f is the voltage line frequency.

The underlying assumption for f_c is that the shaft speed oscillation is periodic with the position of the shaft. Thus, $f_c = f\frac{1-s}{p}$ and the line current $i_s(t)$ is given by the following expression:

$$i_s(t) = v(t)/r(s) \tag{4}$$

where $r(s)$ is the slip-dependent rotor resistance and is expressed as R/s for some nominal resistance R and slip s. The slip s of the motor is defined as

$$s = \frac{N_{sync} - n(t)}{N_{sync}}, \tag{5}$$

where N_{sync} is the synchronous speed of the motor. The synchronous speed N_{sync} can be calculated as

$$N_{sync} = \frac{60}{p} \cdot \frac{\omega}{2\pi}, \tag{6}$$

where ω is the stator electrical frequency in radians per second.

Combining (1) - (6) and using the product of sines trigonometric identity, the line current $i_s(t)$ has a line frequency component which is present from the non-varying speed component of the rotor. The other terms are symmetric sidebands which arise from the shaft speed variation. These shaft speed oscillation harmonics are expressed by

$$f_{sso} = f\left[k\left(\frac{1-s}{p}\right) \pm 1\right], \tag{7}$$

where s is per unit slip, $k = 0, 1, 2...$ and p is the number of pole pairs.

III. Single Motor Environment

To verify the expression in Eq. (7), the following experiment was conducted. A 3 phase, 3 pole-pair ($p = 3$) induction machine is loaded with an evaporator fan in a heating, ventilation and air conditioning (HVAC) unit. Additional weight was placed on the fan to create an imbalance leading to more vibration by adding small weights to a fan blade. A current transducer was placed around one of the phases and thirty seconds of data were recorded for each incremental weight added.

A fast fourier transform (FFT) was taken on the data to compute the spectral content. For this motor, with $p = 3$ and for a low-slip assumption ($s < .05$) and a $f = 60$ Hz supply line frequency, the principal shaft speed oscillation ($k = 1$) is between 79 Hz and 80 Hz. Figure 2 displays the frequency content of the motor for different amounts of weights or clips.

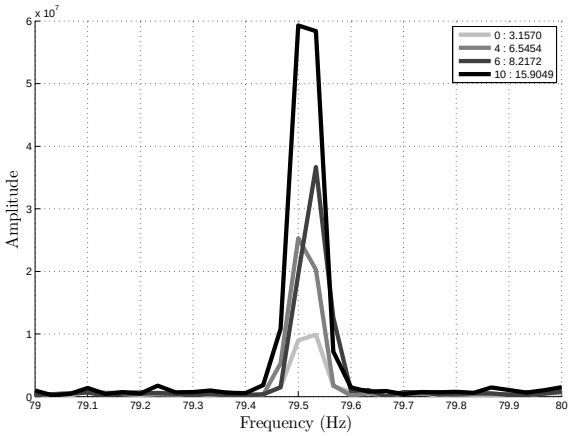

Fig. 2. Energy content of an HVAC evaporator fan for different amounts of weights. More weight leads to more vibration and more energy content from the shaft speed oscillation harmonic.

Table I lists the normalized energy content in the frequency window shown in Fig. 2. The energy is calculated by integrating the total amount of spectral content in the inspection window. The second column displays the reading from an Extech 407860 Heavy Duty Vibration Meter in units of g. The results show that the energy from the shaft speed oscillation harmonic correlates well with radial vibration.

TABLE I
THIS TABLE LISTS THE NORMALIZED ENERGY CONTENT FOR DIFFERENT AMOUNTS OF WEIGHT ADDED.

Number of clips	Vibration Reading (g)	Normalized Energy
0	0.03	3.1570
4	0.09	6.5454
6	0.10	8.2172
10	0.19	15.9049

A second experiment was conducted on a pair of single-phase ventilation fans loaned by the Industrial Electric Shop (IES) on the 1st District Coast Guard base in Boston, Massachusetts. These machines were previously used for intake and exhaust ventilation in the main engine room aboard one of the Coast Guard's 49 ft buoy boats. For these motors, with $p = 1$ and for low-slip assumption ($s < .05$) and a $f = 60$ Hz supply frequency, the principal ($k = 1$) shaft speed oscillation harmonics are between 117 Hz and 120 Hz. To avoid the 120 Hz supply harmonic, the window of inspection included the frequencies between 117 and 119 Hz. Each motor was turned on independently and recorded for 30 seconds.

Figure 3 graphs the frequency content of the intake (3(a)) and exhaust fans (3(b)) for different amounts of weight. Data were taken under "normal" conditions, with a small weight ("little screw") and a larger weight ("big screw") attached to the hub of the fan.

TABLE II
VIBRATION READING AND ENERGY CONTENT OF INTAKE AND EXHAUST VENTILATION FANS UNDER NORMAL CONDITIONS, WITH A LITTLE SCREW AND A BIG SCREW.

	Intake		**Exhaust**	
Eccentric Conditions	Vibration Reading (g)	Norm. Energy	Vibration Reading (g)	Norm. Energy
Normal	0.37	2.8134	0.78	4.0989
Little Screw	0.47	3.4555	1.09	4.3861
Big Screw	0.59	3.9153	1.15	4.6918

Table II lists the normalized energy content in the frequency window for the ventilation fans. The vibration readings were recorded from an Extech 407860 Heavy Duty Vibration Meter in units of g. The results show that the energy from the shaft speed oscillation harmonic correlates well with radial vibration.

IV. Multiple Motor Environment

The previous section demonstrated the effectiveness of using the energy of the shaft speed oscillation harmonic as a measure of radial vibration when only one motor is running on the utility line. This section will extend the algorithm in a multiple motor environment.

A non-intrusive load monitor (NILM) can be used to determine the operating schedule of major electrical loads from measurements taken from a building's electric utility [4, 5]. Dynamic changes in the power and harmonic consumption of a load, e.g., during turn-on or turn-off transients, can serve as a fingerprint for identifying load operation [6, 7].

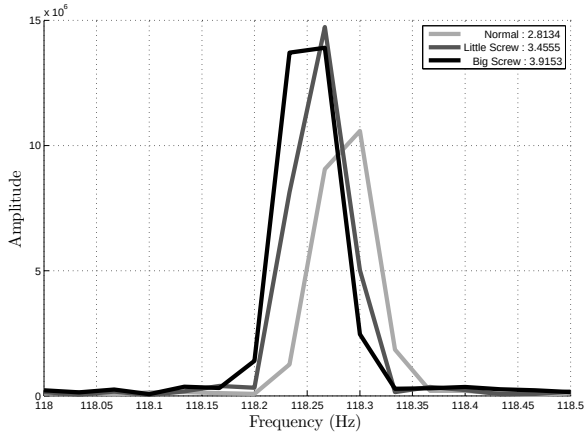

(a)

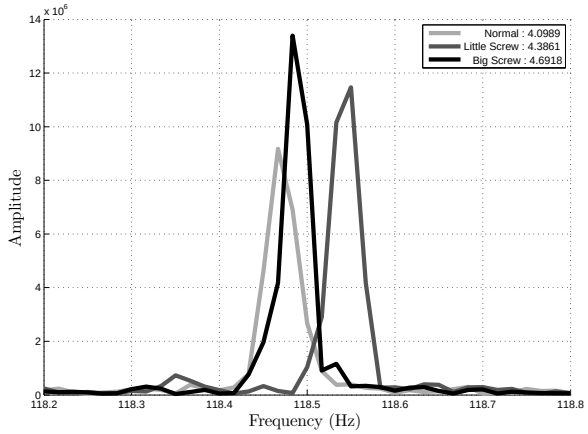

(b)

Fig. 3. Shaft speed oscillation harmonic energy content for intake ventilation fan (a). More eccentric weight correlates with more energy content from the shaft speed oscillation harmonic. The shaft speed oscillation harmonic energy content for the exhaust ventilation fan is shown in (b).

For example, an observed turn-on transient or exemplar from a training observation produced by one of a collection of loads can be used to identify the load in an aggregate current measurement. An analogous procedure can be performed using turn-off transients. All that is needed, in principle, to determine the operating schedule of a collection of loads is to record the aggregate current drawn by those loads and then match each observed transient to the turn-on or turn-off fingerprint of a particular load in the collection.

The NILM was used to detect the speed of a motor in a multi-motor environment using principal slot harmonics [8]. By keeping track of the current and voltage before (pre-trigger) and after (post-trigger) a turn-on transient, the algorithm can estimate the speed of the new load. A similar method is introduced here to estimate the energy content of a shaft speed oscillation harmonic in a multi-motor environment.

The speed estimation method described in [8] calculates the location of the principal slot harmonic. In this paper, the method must calculate the amplitude, or the energy, of the shaft speed oscillation harmonic. This difference leads to a slight modification in how the pre-trigger and post-trigger current spectral information are handled.

Section IV-A will discuss how the method estimates the energy of the shaft speed oscillation harmonic when there is no harmonic from a previous motor in the frequency window of interest. This could mean that there was no motor running prior to a trigger event or it could mean that the speed variation harmonics of previously active motors show up in a different window than the harmonic of the motor causing the trigger event. Section IV-B will discuss how to estimate the energy of the harmonic of a motor in a window when there is another motor with the same number of pole pairs currently running.

A. No Previous Motor

Consider an electrical service feeding a single-phase, single pole-pair intake ventilation fan and the three-phase three pole-pair HVAC evaporator fan described earlier. When the intake ventilation fan is running by itself, there is a speed variation harmonic near 118 Hz described by Eq. (7) as shown in Fig. 4(a). Furthermore, there is no harmonic content near 79 Hz as shown in Fig. 4(b).

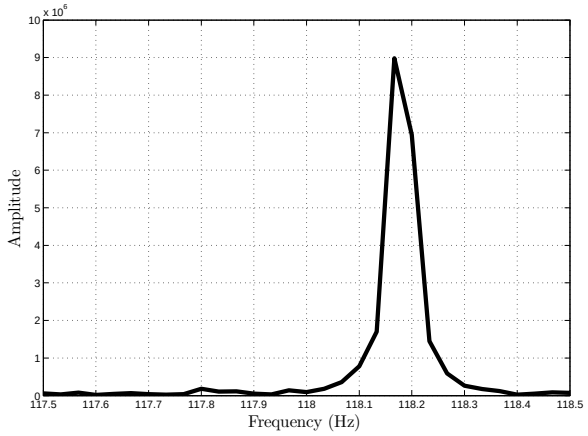

(a)

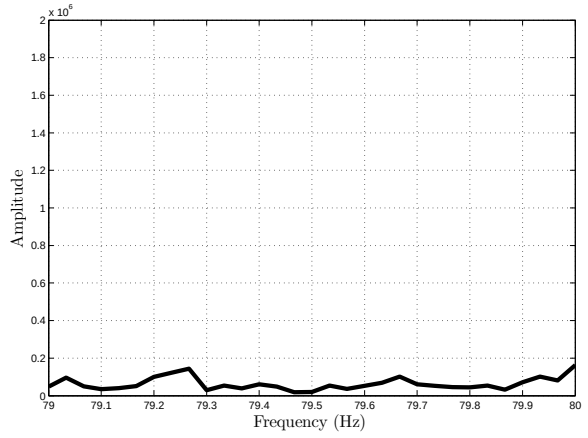

(b)

Fig. 4. Harmonic content of a single phase, $p = 1$ ventilation fan is shown in (a) near 118 Hz but has no harmonic content near 79 Hz (b).

When the HVAC motor turns on, the harmonic content near 118 Hz from the intake ventilation fan is still present in Fig. 5(a) but now there is a spike in the 79 Hz window in Fig. 5(b). The harmonic content near 79 Hz can be thought of as

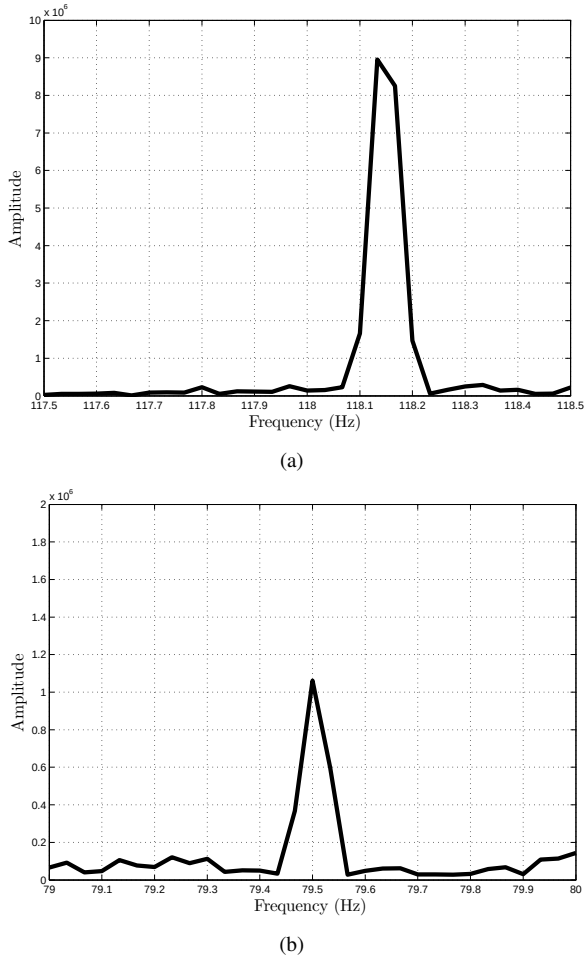

Fig. 5. Harmonic content of a single phase, $p = 1$ ventilation fan and a three phase, $p = 3$ HVAC motor. The $p = 1$ ventilation fan has content near 118 Hz (a) while the $p = 3$ HVAC fan has its harmonic near 79 Hz (b).

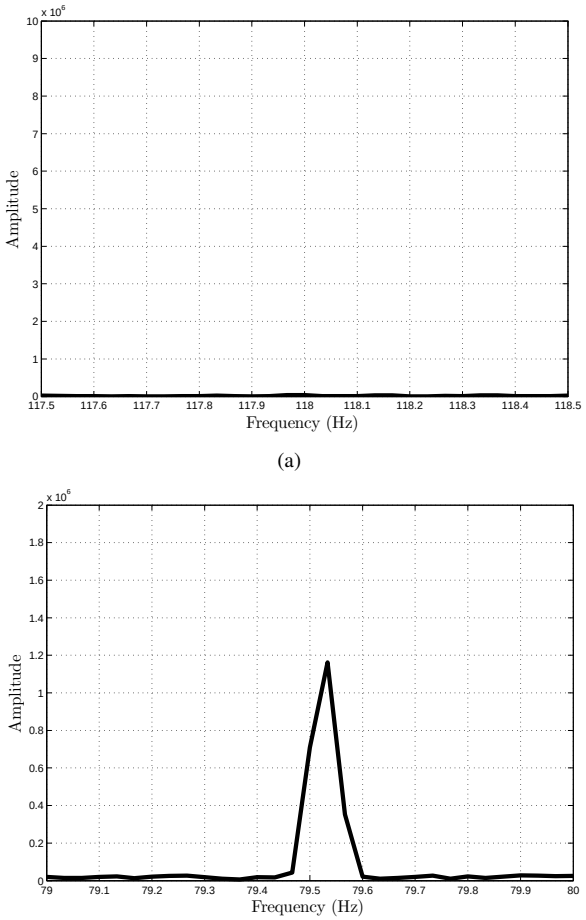

Fig. 6. The three phase, $p = 3$ HVAC fan has no harmonic content near 118 Hz as shown in (a) but has content near 79 Hz (b).

the sum of the content from the intake ventilation fan and the content from the HVAC motor. Figure 6 shows the harmonic content near 118 Hz (a) and 79 Hz (b) when only the HVAC motor was on.

B. Previous Motor

In the case in which there are two speed oscillation harmonics in the same window, the phase between the two harmonics is now a concern, since the method seeks to estimate the amplitude of each harmonic. Consider the following example of two fundamental sinusoids with a relative phase angle of ϕ with frequencies 117.5 and 117.6 Hz, respectively. Let:

$$Y(\phi, t) = \sin(2\pi \cdot 117.5 \cdot t) + \sin(2\pi \cdot 117.6 \cdot t - \phi) \quad (8)$$

be the sum of the two sine waves. Depending on the value of ϕ, the amount of spectral energy contained in a window centered around 117.5 Hz varies. Fig. 7 shows the amount of spectral content in a window between 117 and 118 Hz for several values of ϕ using a 10 second long data record.

As evident in Fig. 7, the energy contained in the window varies depending on the phase difference between the two sinusoids. This fact could lead to an incorrect estimation if the

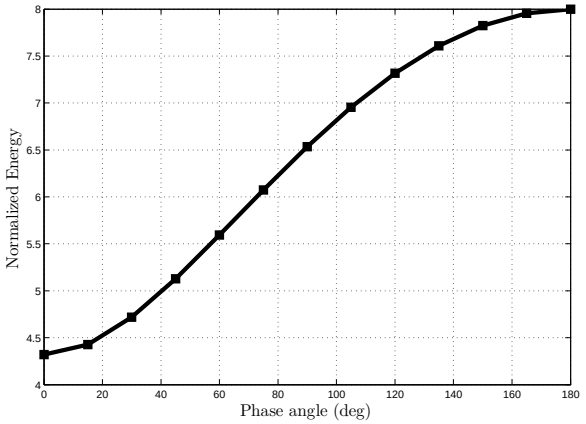

Fig. 7. Energy content of 2 sinusoids with various phase angle difference. The harmonic content energy is a function of this phase difference.

window is not chosen at the appropriate time. Unfortunately, there is no simple way of knowing beforehand when the two shaft speed oscillation harmonics will interfere constructively. To mitigate this problem, tracking the energy over a long enough period with a sliding window will guarantee that eventually these two harmonics will constructively interfere. The following example illustrates this point.

Consider the following scenario involving the intake and exhaust ventilation fans. Assume that the former is running at a slip of s_I with a corresponding shaft speed oscillation harmonic located at f_{ssoI} given by Eq. (7). This harmonic can be modeled as $y_I(t) = \sin(2\pi f_{ssoI} t)$. Now assume that the exhaust ventilation fan is running at a slip of s_E with a harmonic located at f_{ssoE}. The exhaust speed oscillation harmonic is modeled as $y_E(t) = \sin(2\pi f_{ssoE} t - \phi)$ where ϕ is the relative phase angle between $y_I(t)$ and $y_E(t)$.

The algorithm takes advantage of the beat frequency between $y_I(t)$ and $y_E(t)$. If the spectral energy is tracked long enough, the shaft speed oscillation harmonics will be in phase and the energy of each harmonic can be estimated more reliably. As an illustration, assume the intake fan is running at $s_I = 0.0417$ with $f_{ssoI} = 117.5$ Hz. Also, assume the exhaust fan is running at $s_E = 0.04$ with $f_{ssoE} = 117.6$ Hz with a phase angle $\phi = \pi/7$. With a sampling rate of 8000 Hz, a 30 second data record of $y_I(t) + y_E(t)$ is shown in Fig. 8(a). The spectral energy of the shaft speed oscillation harmonics is calculated over a 10 second window. A sliding window with an offset of $T_{offset} = 0.25$ seconds is moved along the entire 30 second window and the spectral energy is calculated in each window.

Figure 8(b) shows the result of the sliding window spectral energy calculation. It is evident that spectral energy is periodic based on the beat frequency between the harmonics. The two peaks in the figure coincide with the alignment of the phases of the two shaft speed oscillation harmonics.

The beat period can be calculated by the following expression

$$T_{beat} = \frac{1}{f_{beat}} = \frac{1}{f\,|s_I - s_E|}, \tag{9}$$

where f is the frequency of the supply line and s_I and s_E are the slips of the intake and exhaust ventilation fans, respectively.

In the previous example with $f = 60$ Hz, $s_I = 0.0417$ and $s_E = 0.04$, the theoretical beat period is $T_{beat-theo} = 9.8$ seconds. Careful examination of Fig. 8(b) shows that the local maxima occur during the 24th and 64th windows, or every $W_{beat} = 40$ windows. With the window offset period of $T_{offset} = 0.25$ seconds, the experimental beat period is $T_{beat-exp} = W_{beat} \cdot T_{offset} = 10$ seconds. If the sampling frequency was faster or if the window offset period was shorter, the error between the theoretical and experimental beat periods would be smaller.

If the slip of the exhaust fan were to decrease to $s_E = 0.0383$, the beat frequency increases and the beat period should decrease. Figure 9 shows the results in which the window beat count has decreased to $W_{beat} = 20$ windows which results in an experimental beat period of $T_{beat-exp} = W_{beat} \cdot T_{offset} = 5$ seconds. The experimental result agrees with the theoretical calculation of $T_{beat-theo} = 4.902$ seconds.

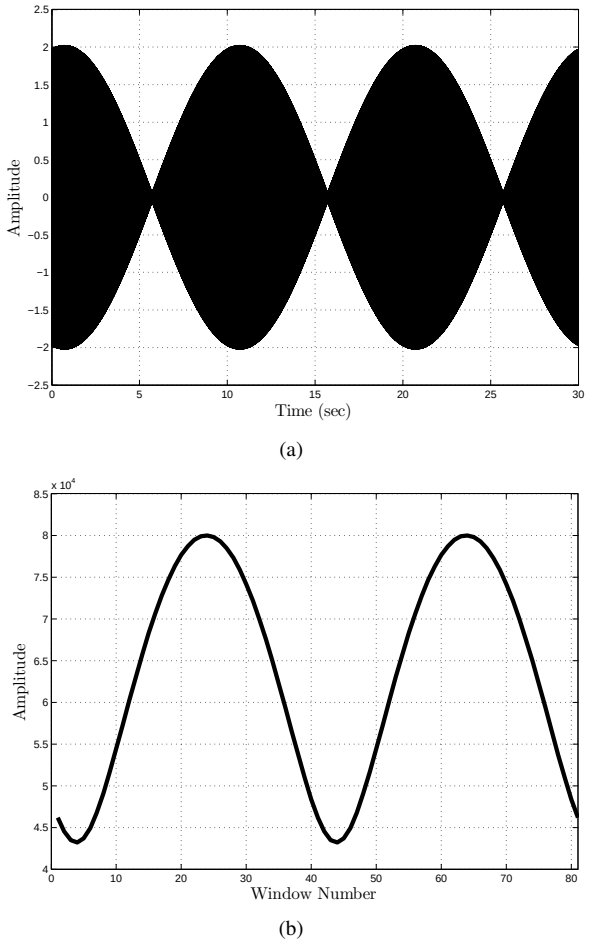

Fig. 8. A plot of two sinusoids with frequencies 117.5 and 117.6 Hz with a phase difference of $\phi = \pi/7$ is shown in (a). The sliding window algorithm shows the beat period of the energy content in (b).

In summary, to compute the energy of a shaft speed harmonic contributed by a motor when there is another motor running with the same number of poles requires an additional amount of work. The sliding window method requires observing the aggregate current signal long enough to detect the first peak. This algorithm breaks down in the unlikely event that both motors are running at identical slip. In this instance, the energy observed is only a function of ϕ_{start}, the phase angle between the two motors the instance the second motor turns on. Since the slip difference between the motors remains constant, the energy from the shaft speed oscillation harmonics will also remain constant.

C. Experimental Results

The theory described in the previous section is applied in the experiments described below. Both the intake and exhaust ventilation fans were used. In the following two experiments, the exhaust fan has no additional weights attached to the fan hub. The intake fan has no additional weight but in the first experiment, an air filter is used to partially block the air flow.

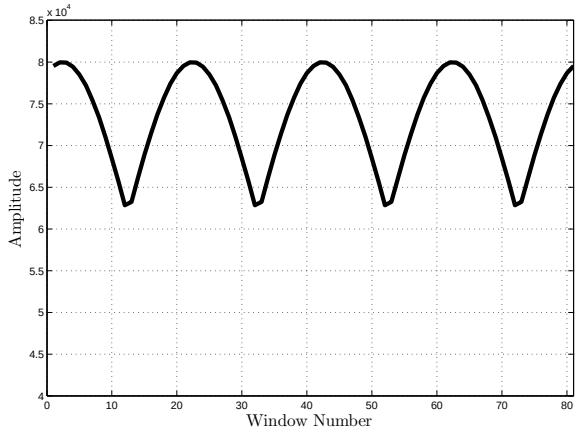

Fig. 9. Sliding window algorithm of 2 sinusoids with slips of .0412 and .0383. With a larger absolute difference in slips between the 2 motors, the beat period has decreased.

In the second experiment, a piece of cardboard filter is used to fully block the air flow to change the slip of the intake fan.

Figure 10 shows the shaft speed oscillation harmonics appearing in the aggregate current. The spectral data shown are taken with a sampling time of 30 seconds and sampling frequency of $f_s = 8000$ Hz. When the intake fan is running by itself, its harmonic is shown in Fig. 10(a). The exhaust fan is later turned on and both harmonics are shown in Figure 10(b). Figure 10(c) contains the shaft speed oscillation when the exhaust fan is on by itself.

Analysis of the principal slot harmonics in Fig. 11 can be used to estimate the speed of any motor [8–13]. When both motors are running, the intake ventilation fan is running at a slip of $s_I = .0249$ and the exhaust ventilation fan is running at a slip of $s_E = .0276$. To get an accurate estimate of the energy of the shaft speed oscillation harmonic from the exhaust fan, the sliding window algorithm mentioned before will have to be used. Equation (9) estimates that the beat period of the oscillation harmonics is $T_{beat-theo} = 6.1728$ seconds. The result from the sliding window algorithm is shown in Fig 12. with a data length of 10 seconds and an offset length of $T_{offset} = 0.25$ seconds.

The two beat periods between the three peaks are 24 and 28 windows, respectively. The experimental beat period in seconds is $T_{beat-exp} = W_{beat} \cdot T_{offset}$. Therefore, the beat period is between 6 and 7 seconds which agrees with the theoretical calculation of 6.1728 seconds. Section IV-D will provide a discussion on the numerical results.

In the second experiment, a blockage of the air intake alters the slip. The shaft speed oscillation harmonics are shown when the intake motor is on by itself (Fig. 13(a)), when both motors are on (Fig. 13(b)) and when the exhaust motor is on by itself (Fig. 13(c)).

Analysis of the principal slot harmonics in Fig. 14 shows that when both motors are running, the intake ventilation fan is running at a slip of $s_I = .0253$ and the exhaust ventilation fan is running at a slip of $s_E = .0271$. The theoretical beat period of the oscillation harmonics is $T_{beat-theo} = 9.2593$ seconds.

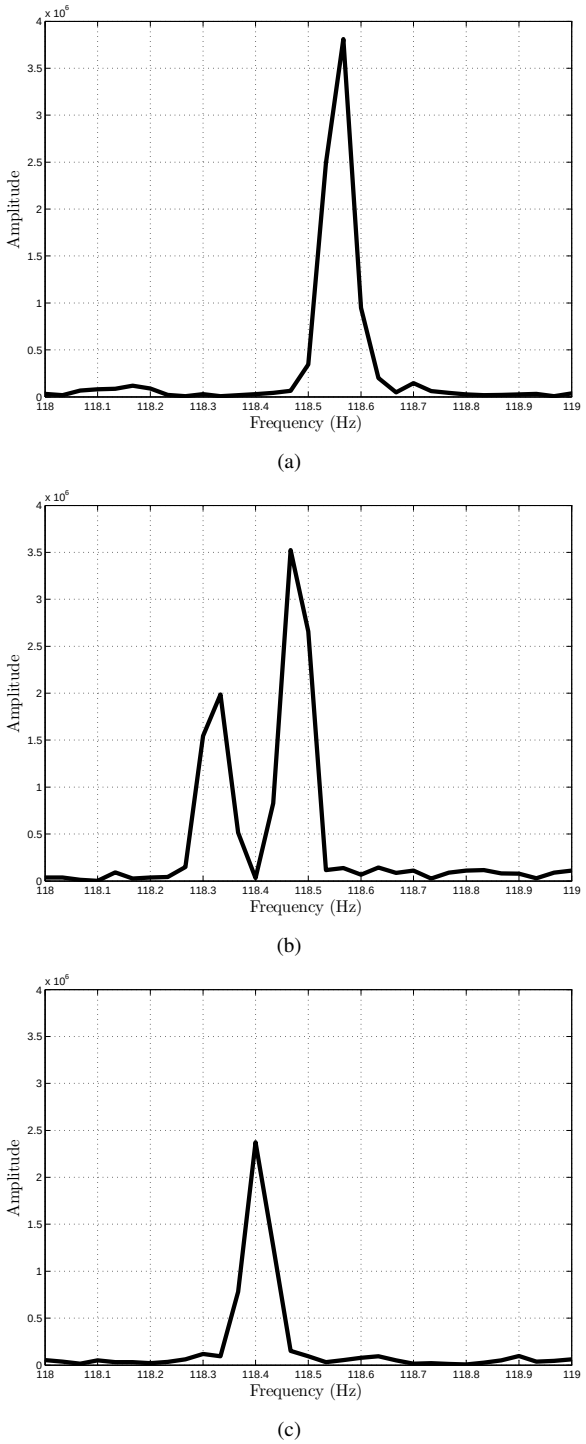

Fig. 10. When the intake ventilation fan runs by itself, its shaft speed oscillation harmonic is shown in (a). The exhaust ventilation fan is then turned on and both oscillation harmonics are shown in (b). The intake ventilation fan is then turned off and the oscillation harmonic of the exhaust fan when running by itself is shown in (c).

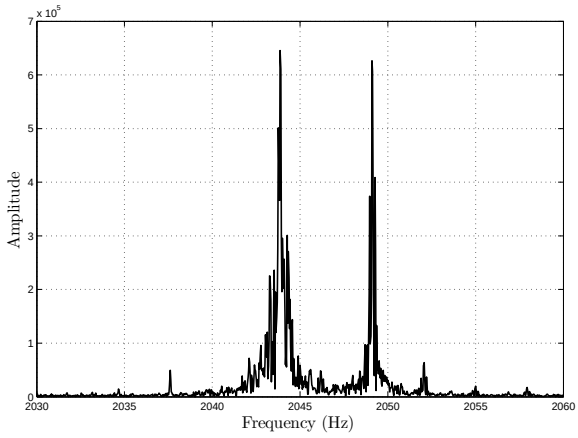

Fig. 11. The principal slot harmonics of the intake and exhaust ventilation fans with an air filter placed over the intake fan. These harmonics can be used to estimate the speeds of each motor.

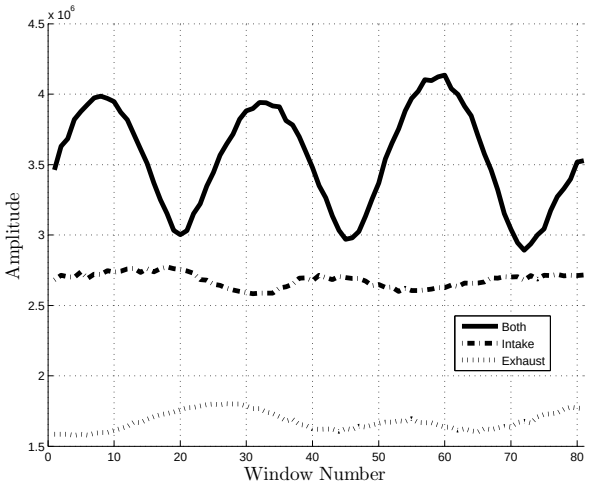

Fig. 12. The bottom two traces show the sliding window algorithm results when the intake and exhaust ventilation fans are running by themselves. The top trace shows the sliding window when both fans are on. The harmonic energy content is periodic and the period can be determined from calculating the slips of each fan.

The results from the sliding window algorithm is shown in Fig. 15. The beat period in window counts between the two peaks is 37 which results in an experimental beat period $T_{beat-exp}$ of 9.25 seconds. Both the theoretical and experimental beat periods agree with one another.

D. Slip Difference

One limitation facing the vibration monitoring algorithm deals with the slip changes that occur when both ventilation fans are running at the same time. When both motors are loading the utility line, the voltage amplitude drops and this slows down the motors. This slip difference also changes the total energy content from the shaft speed oscillation harmonic. One possible explanation is when the slip changes, the motor is operating at a new point on its torque-speed curve. Each point on the curve may react differently to eccentric weight depending on the torque turning the shaft. Another explanation for the change in harmonic content is that the circuit model in

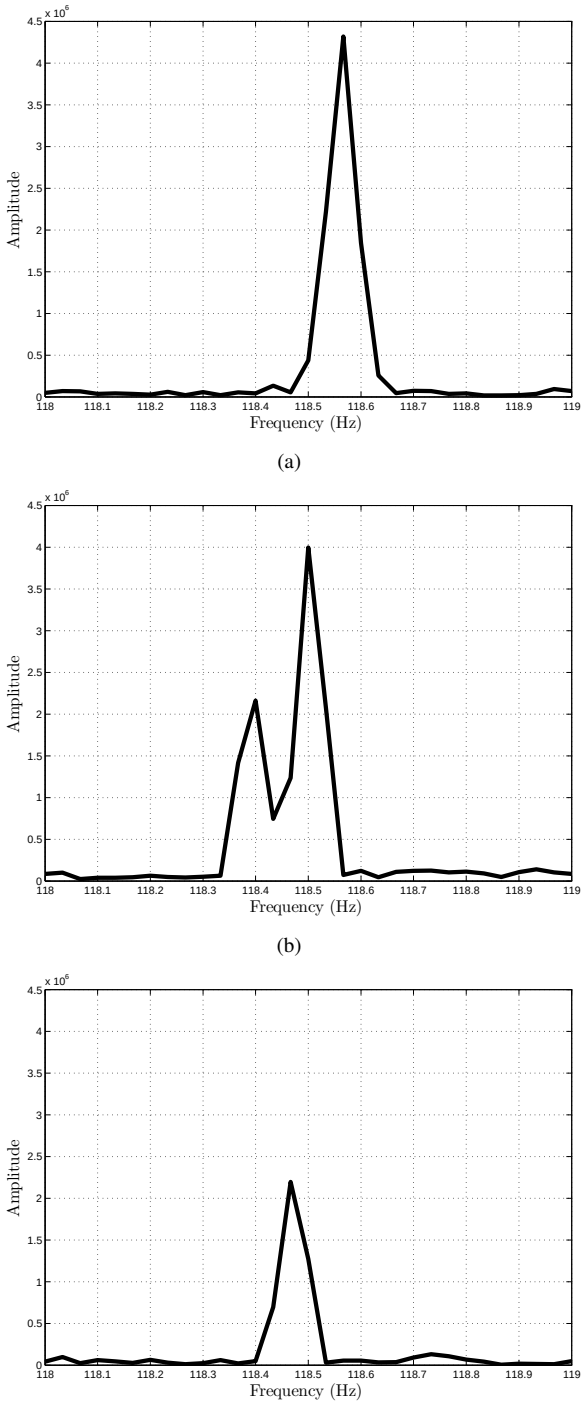

Fig. 13. When the intake ventilation fan runs by itself with a higher slip, its shaft speed oscillation harmonic is shown in (a). The exhaust ventilation fan is then turned on and both oscillation harmonics are shown in (b). The intake ventilation fan is then turned off and the oscillation harmonic of the exhaust fan when running by itself is shown in (c).

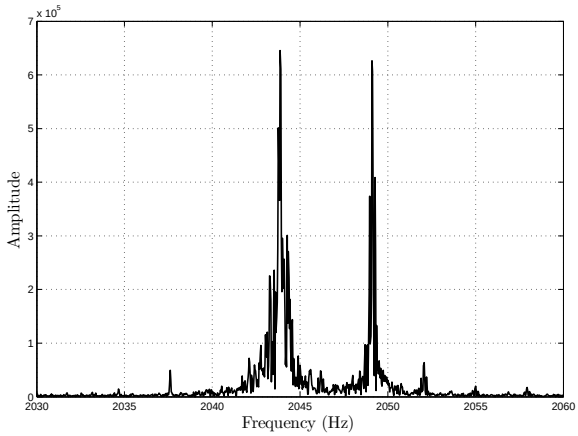

Fig. 14. The principal slot harmonics of the intake and exhaust ventilation fans with cardboard placed over the intake fan. These harmonics can be used to estimate the speeds of each motor.

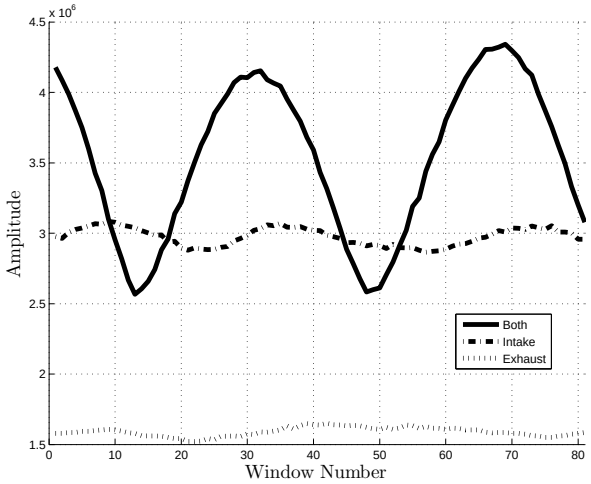

Fig. 15. The bottom two traces show the sliding window algorithm results when the intake and exhaust ventilation fans are running by themselves. The intake fan's airflow is blocked by a piece of cardboard. The top trace shows the sliding window when both fans are on. The harmonic energy content is periodic and the period can be determined from calculating the slips of each fan.

Fig. 1 includes a slip-dependent resistance. If the slip changes, then the amplitude of the current will also change.

Table III shows how the slip differs for the intake and exhaust ventilation fans when each is running by itself versus when they are running at the same time.

TABLE III
SLIP CHANGES FOR THE INTAKE AND EXHAUST VENTILATION FANS. AS SHOWN, THE SLIP INCREASES (SPEED DECREASES) FOR EACH MOTOR WHEN BOTH ARE TURNED ON.

	Experiment 1 Filter		Experiment 2 Board	
Segment	Intake	Exhaust	Intake	Exhaust
Intake Only	.0237	–	.0242	–
Exhaust Only	–	.0260	–	.0259
Intake + Exhaust	.0249	.0276	.0253	.0271

Table IV shows the total amount of energy in the window in which the shaft speed oscillation harmonic is located. Recall that Experiment 1 had an air filter placed over the intake fan while Experiment 2 had a cardboard blocking the airflow over the intake fan. The expected sum is the sum of the first 2 columns, the energy content from each fan when they are running by themselves. The observed sum is the actual observed energy content. The results show that there is some error in estimation. If the exhaust ventilation fan's vibration had to be estimated assuming the intake's vibration is as enumerated in column 1, then the estimate would be higher than the true value. To circumvent this problem, the algorithm could have a baseline reading for each motor under all the possible permutations. There would be a baseline vibration reading for the intake fan when it runs by itself and when it runs with the exhaust fan running concurrently. Two similar baseline readings would need to be recorded for the exhaust fan.

TABLE IV
THIS TABLE SHOWS THE ENERGY CONTENT OF EACH FAN WHEN THEY ARE RUNNING BY THEMSELVES. IT ALSO SHOWS THE ERROR BETWEEN THE EXPECTED ENERGY CONTENT WHEN BOTH ARE RUNNING AND THE OBSERVED.

	Intake	Exhaust	Expected Sum	Observed Sum
Experiment 1	2.6796	1.6787	4.3583	4.1344
Experiment 2	2.9756	1.5902	4.5658	4.3411

V. FUTURE WORK

Another potential for electrical-based condition monitoring comes from the outer and inner race frequencies caused by bearing failures. An initial study was study done to investigate the "efficacy of current monitoring for bearing fault detection by correlating the relationship between vibration and current frequencies caused by incipient bearing failures" [14]. Further work looks to analyze how ball-bearing frequencies can provide additional metrics to monitor vibration in addition to the shaft speed oscillation harmonics and how effective these methods are outside of a lab environment. These electrical-based condition monitoring methods will be tested on board the USCGC Escanaba but there are other considerations that need to be analyzed before these algorithms can be fully implemented in the field. Ventilation duct fans on board the ship are mounted in ducts and the stiffness of the mounting can affect the reliability of the ball-bearing frequencies.

A. Effect of Fan Mounting Stiffness

Ducted fans all contain three parts: a fan, a motor, and the duct pipe section. The fan is rigidly attached to the shaft of the motor forming the fan/rotor assembly. The fan/rotor assembly is secured axially and radially to the motor by a pair of deep grove ball bearings. Ball bearings, primarily through the flexibility of their constituent materials, possess a radial stiffness that can be modeled as a linear spring and damper in parallel. The motor body in a ducted fan is rigidly attached to the duct pipe section, while the duct pipe section is often attached to low stiffness but highly dampening vibration isolation mounts which secure the unit to the surrounding structure.

Fan imbalance faults occur when the center of mass of a fan rotor assembly is not coincident with the center of rotation of the assembly. These faults can be easily induced in the lab by attaching a small mass to a given fan blade of an otherwise balanced or fault free fan assembly. The presence of an eccentric weight of mass m attached at radius r from the axis of rotation gives rise to an imbalance force F described acting on the rotor fan assembly.

$$F_i = m_i \omega^2 r \sin(\omega t)$$

Assuming that the mass of the rotor assembly is very much larger than the imbalance mass ($m_r >> m_i$), the equations representing the radial motion of the fan/rotor assembly and the motor stator/ duct pipe assembly are given as follows for the x or y direction (perpendicular to the axis of the fan):

$$\begin{aligned} m_d \ddot{x_d} &= -x_d k_m - \dot{x_d} b_m + (x_r - x_d) k_b \\ &\quad + (\dot{x_r} - \dot{x_d}) b_b \\ m_r \ddot{x_r} &= -(x_r - x_d) k_b - (\dot{x_r} - \dot{x_d}) b_b + F_i \end{aligned}$$

The meaning of the variables above may be deduced from the following figure.

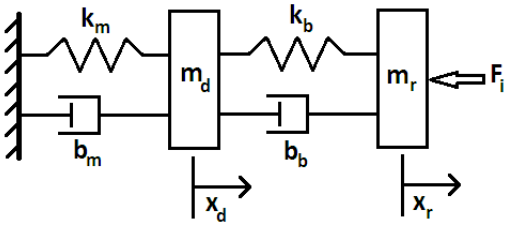

Fig. 16. Mass Spring Damper model used to illustrate the effect of stiffness on the electric detection metric.

Electrical detection methods for imbalance related faults in an induction motor rely on the relative radial motion of the rotor and stator: $(x_r - x_d)$. In un-faulty situations a balanced rotor runs true and its radial clearance is kept uniform by the bearing stiffness. However an imbalanced rotor will exert the F_i reaction force on the bearing causing a vibration in the radial direction. The bearing will flex under the imbalance force and a point of minimum radial distance between the inner race and the outer race will form and this point is fixed with respect to the inner race. As the balls of the bearing roll past this point, they will cause a periodic disturbance/variation in the rotational friction coefficient of the bearing. This periodic variation in the rotation friction will occur at the bearing's inner race ball pass frequency. The variation in friction will also cause a periodic rotor speed variation, and this speed variation will show up in the current signature of the motor at the same frequency. This is the basis for the electrical detection method. A metric of electrical sensitivity to imbalance is the amplitude of $(x_r - x_d)$. This metric happens to be sensitive to the properties of the vibration isolation mount, specifically its stiffness k_m. For appropriate scaling of all parameters i.e $m_d \approx m_r$ and $k_b >> k_m$, one can get the following behavior of the electric detection metric as shown in Fig. 17.

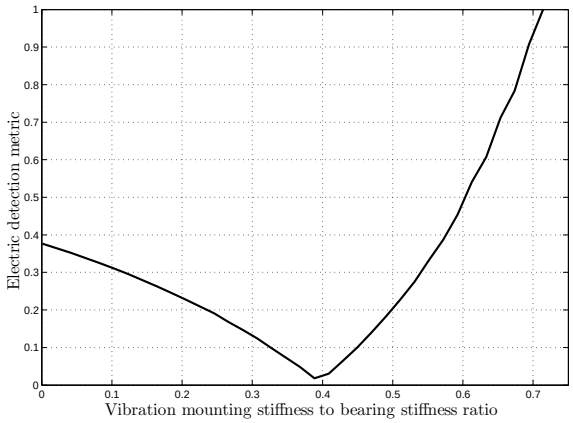

Fig. 17. The effect of mounting stiffness on the electric detection metric. It can be seen that the detection metric is sensitive to the vibration mounting stiffness.

The rise in the metric toward the right end of the plot is a resonance associated with the specific excitation frequency chosen. It can be seen that the detection metric is sensitive to the vibration mounting stiffness.

VI. Conclusions

This paper has demonstrated that the shaft speed oscillation harmonics can serve as an electrical-based vibration reading for monitoring the health of motors. Result from experiments in a laboratory environment were consistent with this claim. Furthermore, an algorithm was developed that could allow for diagnostics of two loads from one aggregate current signal. There are some limitations to these methods. It was shown that two loads running off the same utility may cause the slips of each load to decrease. A robust algorithm will need to take this phenomenon into consideration. Further work looks to analyze how ball-bearing frequencies can be used to monitor vibration in addition to the shaft speed oscillation harmonics.

VII. Acknowledgments

This work was supported in part by the ONR ESRDC program, The Grainger Foundation and the BP-MIT Research Alliance.

References

[1] E. Linton, "Coast Guard RCM/CBM Initiatives." Presented at the 2005 Department of Defense Maintenance Symposium and Exhibition, Birmingham, AL, Oct. 2005.

[2] W. T. Thomson, R. A. Leonard, A. J. Milne, and J. Penman, "Failure Identification of Offshore Induction Motor Systems Using On-condition Monitoring," *Reliability Engineering*, vol. 9, no. 1, pp. 49–64, 1984.

[3] G. B. Kliman and J. Stein, "Methods of Motor Current Signature Analysis," *Electric Machines and Power Systems*, vol. 20, no. 5, pp. 463–474, 1992.

[4] S. B. Leeb, "A Conjoint Pattern Recognition Approach to Nonintrusive Load Monitoring," Ph.D. dissertation, Massachusetts Institute of Technology, Cambridge, MA, Feb. 1993.

[5] S. B. Leeb, S. R. Shaw, and J. L. Kirtley Jr., "Transient Event Detection in Spectral Envelope Estimates For Nonintrusive Load Monitoring," *IEEE Trans. Power Del.*, vol. 10, no. 3, pp. 1200–1210, Jul 1995.

[6] S. R. Shaw, S. B. Leeb, L. K. Norford, and R. W. Cox, "Nonintrusive Load Monitoring and Diagnostics in Power Systems," *IEEE Trans. Instrum. Meas.*, vol. 57, no. 7, pp. 1445–1454, Jul. 2008.

[7] S. R. Shaw, "System identification techniques and modeling for nonintrusive load diagnostics," Ph.D. dissertation, Massachusetts Institute of Technology, Cambridge, MA, Feb. 2000.

[8] U. A. Orji, Z. Remscrim, C. Laughman, S. B. Leeb, W. Wichakool, C. Schantz, R. Cox, J. Paris, J. L. Kirtley, and L. K. Norford, "Fault Detection and Diagnostics for Non-Intrusive Monitoring Using Motor Harmonics," in *Applied Power Electronics Conference and Exposition (APEC), 2010 Twenty-Fifth Annual IEEE*, Feb. 2010, pp. 1547–1554.

[9] K. D. Hurst and T. G. Habetler, "Sensorless Speed Measurement Using Current Harmonic Spectral Estimation in Induction Machine Drives," *IEEE Trans. Power Electron.*, vol. 11, no. 1, pp. 66–73, 1996.

[10] A. Ferrah, K. G. Bradley, and G. M. Asher, "Sensorless Speed Detection of Inverter Fed Induction Motors Using Rotor Slot Harmonics and Fast Fourier Transform," vol. 1. IEEE Power Electronics Specialist Conference, Jun. 29 - Jul. 3 1992, pp. 279–286.

[11] A. Ferrah, P. J. Hogben-Laing, K. J. Bradley, G. M. Asher, and M. S. Woolfson, "The Effect of Rotor Design on Sensorless Speed Estimation Using Rotor Slot Harmonics Identified by Adaptive Digital Filtering Using The Maximum Likelihood Approach," in *Industry Applications Conference, 1997. Thirty-Second IAS Annual Meeting, IAS'97., Conference Record of the 1997 IEEE*, vol. 1, Oct. 1997, pp. 128–135.

[12] A. Ferrah, K. J. Bradley, P. J. Hogben-Laing, M. S. Woolfson, G. M. Asher, M. Sumner, J. Cilia, and J. Shuli, "A Speed Identifier For Induction Motor Drives Using Real-Time Adaptive Digital Filtering," *IEEE Trans. Ind. Appl.*, vol. 34, no. 1, pp. 156–162, 1998.

[13] K. D. Hurst and T. G. Habetler, "A Comparison of Spectrum Estimation Techniques For Sensorless Speed Detection in Induction Machines," *IEEE Trans. Ind. Appl.*, vol. 33, no. 4, pp. 898–905, 1997.

[14] R. R. Schoen, T. G. Habetler, F. Kamran, and R. G. Bartfield, "Motor Bearing Damage Detection Using Stator Current Monitoring," *IEEE Trans. Ind. Appl.*, vol. 31, no. 6, pp. 1274–1279, 1995.